

Large-Eddy Simulation of Air Pollution Dispersion in the Nocturnal Cloud-Topped Atmospheric Boundary Layer

Zbigniew Sorbjan¹ and Marek Uliasz²

¹ Marquette University, Milwaukee, WI 53201, e-mail: sorbjanz@mu.edu,

² Mission Research Corporation, ASTER Division, 2629 Redwing Rd, Suite 310, Fort Collins, CO 80523
e-mail: uliasz@aster.com

Abstract. Effects of stratocumuli clouds on dispersion of contaminants are studied in the nocturnal atmospheric boundary layer. The study is based on a large-eddy simulation (LES) model with a bulk parametrization of clouds. Computations include Lagrangian calculations of atmospheric dispersion of a passive tracer released from point sources at various heights above the ground. The obtained results show that the vertical diffusion is non-Gaussian and depends on the location of a source in the boundary layer.

1. INTRODUCTION

During the last three decades, a good understanding of atmospheric diffusion has been achieved in the convective boundary layer as a result of numerical, laboratory, and field investigations (e.g., Weil, 1995). All previous studies, however, have focused on day-time, clear-sky convection over land, and consequently either eliminated or simply ignored convection due to the presence of low clouds at the top of the boundary layer. Low, stratocumuli clouds, especially in nocturnal conditions, are able to generate a rather strong convection (e.g., Garratt, 1992), and therefore can have an important impact on the structure of atmospheric turbulence and diffusion.

Due to a positive vertical velocity skewness in convective boundary layer (CBL), dispersion during the day-time depends on the location of the source. As a result, dispersion from a source located near the Earth's surface is different than dispersion from a source at the top of the boundary layer. On the other hand, the skewness in the cloud-topped boundary layer (CTBL) is generally negative. Consequently, dispersion in the CTBL is also expected to be dependent on the location of the source, but in a "reverse" way.

In order to evaluate this notion, we performed a preliminary test based on a large-eddy simulation (LES) model. Our large-eddy simulation model is briefly described in Section 3. In Section 2, we discuss the differences and similarities between convection in the clear-sky convective boundary layer and in the cloud-topped boundary layer. The results of our numerical simulations are detailed in Section 4.

2. CONVECTIVE DIFFUSION

2.1. Surface-generated convection

Diffusion of pollutants in the clear-sky convective boundary layer is primarily governed by turbulence generated by surface heating. The understanding of diffusion in the CBL was significantly advanced by the numerical simulations and laboratory experiments of Willis and Deardorff (1976, 1978, 1981). These investigations demonstrated that for elevated sources, the average plume center-line, defined as the mean maximum concentration, descended within a short distance from the source until it reached the ground. In contrast, the average centerline from near surface releases ascended after a short downwind distance.

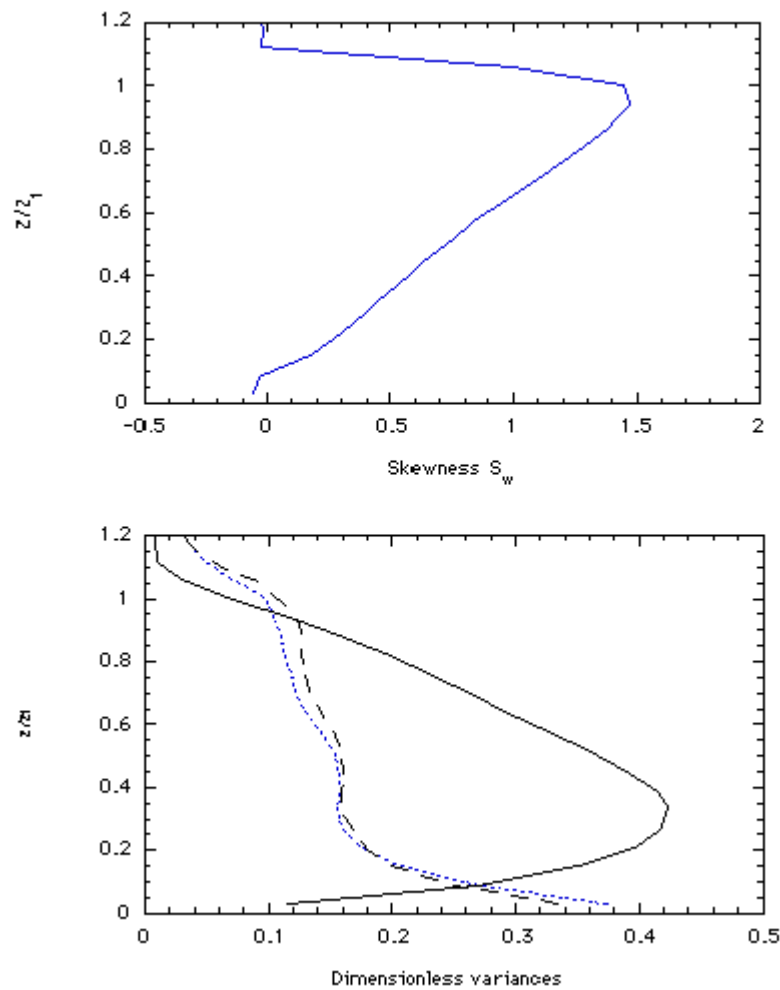


Figure 1: Vertical profiles of (a) the vertical velocity skewness, and (b) dimensionless velocity variances (scaled by w_*^2) in the CBL: u-dotted line, v - dashed line, w - continuous line.

This rather surprising plume behavior strongly differed from the conclusions of the Gaussian plume models. After many subsequent studies, it became clear that the position of maximum concentrations can be explained by the probability distribution of the vertical velocity. Such distribution was found to be positively skewed, with a negative mode in the CBL (e.g., LeMone, 1990). A typical example of the vertical velocity skewness ($Sw = \langle w'^3 \rangle / \langle w'^2 \rangle^{3/2}$) in the CBL is shown in Figure 1. In the same figure, dimensionless vertical profiles of the velocity variances ($\langle u'^2 \rangle$, $\langle v'^2 \rangle$, $\langle w'^2 \rangle$) are also depicted. The figure was generated by our LES model for the case of pure convection (no wind), with the convective velocity scale $w_* = 0.93$ m/s, and the mixing height $h = 495$ m. The velocity variances in Figure 1 are normalized by the convective scale w_* . The resulting skewness near the surface is weakly negative, as a result of insufficient resolution of small eddies in this region by LES models.

A positive vertical velocity skewness indicates strong narrow updrafts surrounded by larger areas of weaker downdrafts. It also implies that downdrafts cover more than half the area of the horizontal plane over the bulk of the mixed layer depth. As a result, the majority of material released by an elevated source descends. On the other hand, material released at the surface can only ascend or move horizontally. Contaminants released into the base of an updraft begin to rise immediately, while those emitted into a downdraft move horizontally until they encounter updrafts. After a sufficiently long travel time, most pollutants enter the updrafts and the location of the maximum concentration rises toward the top of the mixed layer.

The first support for Willis and Deardorff's laboratory observations was obtained from the numerical experiments of Lamb (1982). Lamb used the results from Deardorff's LES model (1972) to trace the motions of thousands of particles released into a numerical field. Laboratory and numerical results were later found to be in a very good agreement with atmospheric observations (e.g., Moninger and Kropfli, 1982, Eberhart et al., 1988).

2.2. Cloud-generated convection

Low clouds have a strong impact on the dynamics of the ABL (e.g., Lenschow et al. 1980, Nichols and Leighton 1986, Turton and Nicholls 1987, Paluch and Lenschow 1991). The structure of the cloud-topped boundary layer depends on the surface sensible and latent fluxes, radiative cooling and heating in clouds, phase changes, subsidence, and wind shear. Surface fluxes generate convection and provide the water substance. Radiative cooling contributes to the generation of a positive heat flux, convection, and entrainment at the top of the mixed layer. Wind shear increases entrainment. Entrainment brings warmer and drier air down into the ABL and promotes evaporative cooling. The evaporative cooling can lead to an instability process whereby parcels cool even more and then sink. This can generate greater entrainment and result in the breaking up of a solid cloud deck.

The day-time CTBL usually has two distinct layers, the cloud and sub-cloud layer, decoupled by the formation of a slightly stable layer near the cloud base. The decoupling is primarily a consequence of short wave heating in the cloud layer. The decoupling prevents the moisture to be transported upward. This, together with solar heating, leads to a rapid thinning of the cloud layer during the daytime, and also has an important influence on the radiative balance at the surface and above the cloud. In addition, cooling introduced by the evaporation of precipitation (drizzle) can cool the sub-cloud layer relative to the cloud layer, and consequently further stabilize the interface between the cloud and sub-cloud layers. Observations reveal negative values of the vertical velocity skewness through a considerable depth within the cloud layer in a daytime boundary layer (e.g., Nicholls and Leighton, 1986).

The CTBL at night is characterized by more intensive turbulence than during the day. The nocturnal CTBL is primarily driven by evaporative and long-wave cooling from the cloud top, in a manner analogous to that of a convective boundary layer heated from below. It gives the appearance of a single mixed layer.

We will focus on the nocturnal CTBL in this study. Typical examples of the vertical velocity skewness and the velocity variances and from the LES in a nocturnal CTBL are shown in Figure 2. The velocity variances in Figure 2b are not normalized. The corresponding profiles of temperature, humidity and fluxes, obtained for the case displayed in Figure 2 are shown in Figures 3, 4 and 5. Figure 3 indicates that the generated cloud extends from about 200 m to 800 m above the ground. The maximum of the vertical velocity variance in Figure 2b is equal to $0.28 \text{ m}^2/\text{s}^2$. For comparison, the maximum of the vertical velocity variance derived from Figure 1b (day-time convection) is about $0.33 \text{ m}^2/\text{s}^2$.

Figure 2 implies negative values of the vertical velocity skewness in the boundary layer, except near the cloud top in the nocturnal CTBL, where the skewness is positive. Negative skewness in the CTBL implies strong narrow downdrafts, surrounded by larger areas of weaker updrafts. Moeng and Rotunno (1990) argued that the cloud-top positive maximum in vertical velocity skewness could be the result of the updrafts impinging upon the inversion and producing weak broadly distributed return flow downdrafts. The positive values of the skewness in Fig. 2 near the cloud top could partly result from the insufficient resolution in this region (in the case shown in Figure 2, the vertical grid sizes $\Delta z=30 \text{ m}$).

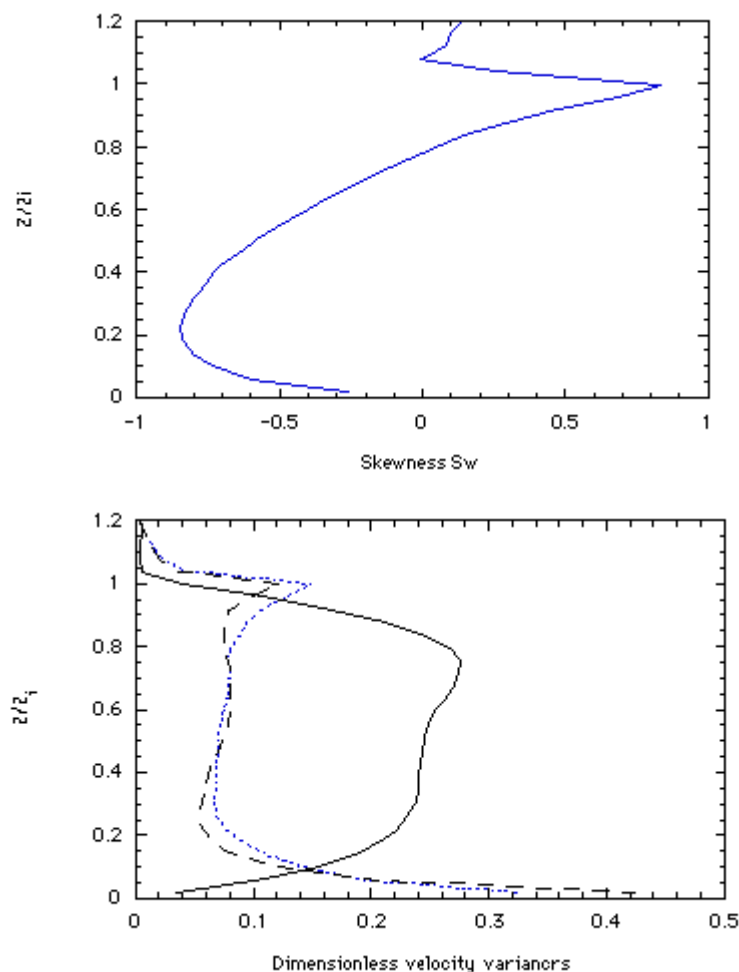


Figure 2. Vertical profiles of (a) the vertical velocity skewness, and (b) dimensionless velocity variances (scaled by w_*^2) in the CTBL: u - dotted line, v - dashed line, w - continuous line.

3. NUMERICAL SIMULATIONS

3.1. LES model

Our study is based on a large-eddy simulation model. LES models are presently considered to be reliable sources of turbulent data, especially because of the known difficulties with assembling high resolution data bases on atmospheric turbulence (e.g., Nieuwstadt et al., 1992). They use equations which remain faithful to the essential physics of the flow and directly resolve most of the turbulence from the Navier-Stokes equations. Only the small scale turbulence is modeled (e.g., Nieuwstadt, 1990, Mason, 1994). LES models have now the capability to produce details down to scales, which are comparable with the scales measured from aircraft (Nichols, 1989). The first large-eddy simulations were performed by Deardorff (1972; 1973; 1974), and were later investigated by e.g., Schemm and Lipps (1976), Sommeria (1976), Moeng (1984), Wyngaard and Brost (1984), Schmidt and Schumann (1989), Mason (1989). Much of the previous work based on LES has been focused on simulations of the convective boundary layers (Nieuwstadt et al., 1992). The cloudy boundary layers were simulated by e.g., Sommeria 1976; Deardorff 1980; Moeng 1986; Moeng et al. 1996; Lewellen and Lewellen 1996, Cuijpers and Duynkerke (1993).

The results presented in this paper are based on the LES model of Sorbjan (1996) with a bulk parametrization of clouds (e.g., Deardorff, 1980, Cuijpers and Duynkerke, 1993). The code was previously used to study the cloud-free convective mixed layer (e.g., Sorbjan, 1995, 1996 a, b). The model employs a system of differential equations consisting of conservation laws for momentum, mass, and the first law of thermodynamics. The unknown quantities include the three components of velocity, the liquid water potential temperature, total water specific humidity, and pressure. The adopted sub-grid parametrization is based on the kinetic energy equation. The Monin-Obukhov similarity formulation is employed to calculate surface momentum fluxes. The upper boundary condition is assumed to be stress-free for horizontal velocity components. At the top of the computational domain, the vertical velocity is set on zero, and the potential temperature lapse rate is constant. The multi-stage Runge-Kutta scheme is used for time integration of all model equations. The monotonic advection scheme of Beets and Koren (1996) is applied for scalar equations.

3.2. Lagrangian particle model

Numerical simulations of turbulent dispersion can be carried out with the help of both, the Eulerian and Lagrangian methods. The Eulerian method is based on the diffusion equation derived from the mass conservation principle. In this case, the diffusion equation is solved along with other conservation equations of the LES model. In the Lagrangian method, “marked” fluid particles are advected in the flow fields (resolved and subgrid) calculated by the LES model. The Lagrangian modeling framework was employed in this study.

Our Lagrangian particle model is designed to evaluate Lagrangian turbulence statistics and to investigate source-receptor relationships from the LES output. It has evolved from a family of particle dispersion models used in mesoscale and regional transport studies (Uliasz, 1994, Uliasz et. al., 1996). Each particle is tagged with the time and location of its release and, additionally, can also be used to trace any meteorological field along its trajectory. The equation of motion for the particle is integrated by a second-order Runge-Kutta scheme (Yeung and Pope, 1988). Resolvable scale wind components from the LES are interpolated linearly to the particle position. Below the $Dz/2$ level, u and v components are derived with the aid of the Monin-Obukhov similarity profiles. Subgrid scale velocity components are generated with the simple random walk scheme. The particle model is formulated as a subroutine called on each time step of integration of the LES code.

Under the assumption of statistical stationarity and horizontal homogeneity of the LES fields in this study, the probability density function for the ensemble mean concentration from a point source takes on the following form:

$$p(x, y, z, t | x', y', z', t') = f(x - x', y - y', z, t - t'),$$

where p is the probability that particle released at the source coordinates (x, y, z) at the time t reaches the receptor coordinates (x', y', z') at the time t' , and f indicates a function of horizontal travel distances $x - x'$, $y - y'$ (due to horizontal homogeneity), travel time $t - t'$ (due to steady state), source height, z , and receptor height, z' .

Particles are being released continuously from randomly selected points at the horizontal plane corresponding to the emission source height. This source area covers the entire LES model domain, while particles are traced in a much larger domain, taking into account the horizontal periodicity of the meteorological fields. The particle simulation starts after the LES solution has reached the steady state. Finally, the ensemble mean concentration is evaluated from the stored particle distributions as a function of $(x - x', y - y', z)$. The uniform kernel estimator (Uliasz, 1994) with bandwidths equal to a half of the assumed grid spacings is used in concentration calculations.

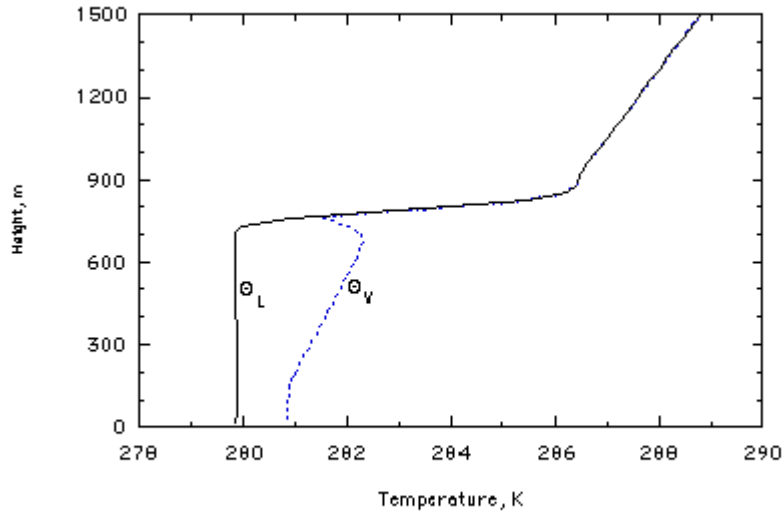


Figure 3. Vertical profiles of the potential liquid water temperature Q_L , and the virtual temperature Q_v for the CTBL simulation.

3.3. Resulting meteorological fields

Our preliminary simulation employed a coarse mesh of $32 \times 32 \times 60$ grid points, distanced at $\Delta x = 60$ m, $\Delta y = 60$ m, and $\Delta z = 30$ m. The heat flux at the surface was nil. A surface humidity flux was 10^{-5} m/s. The geostrophic wind was assumed to be 2 m/s. The lapse rate in the free atmosphere was assumed 3 K/km. The

roughness length was 0.1 m. The absorber layer at the top of the computational domain was located above 2400 m. Its time constant was assumed to be 1000 s. The simulation lasted 15,136 s.

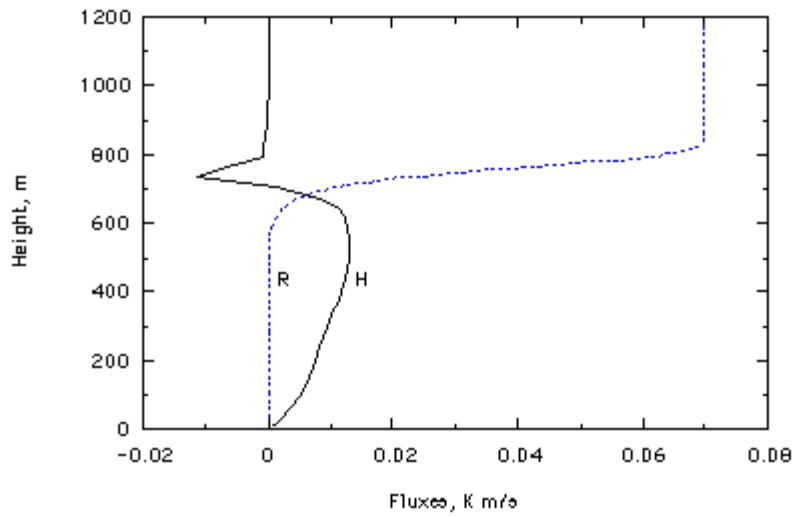


Figure 4. Vertical profiles of the turbulent (total) heat flux H , and the net radiative flux R .

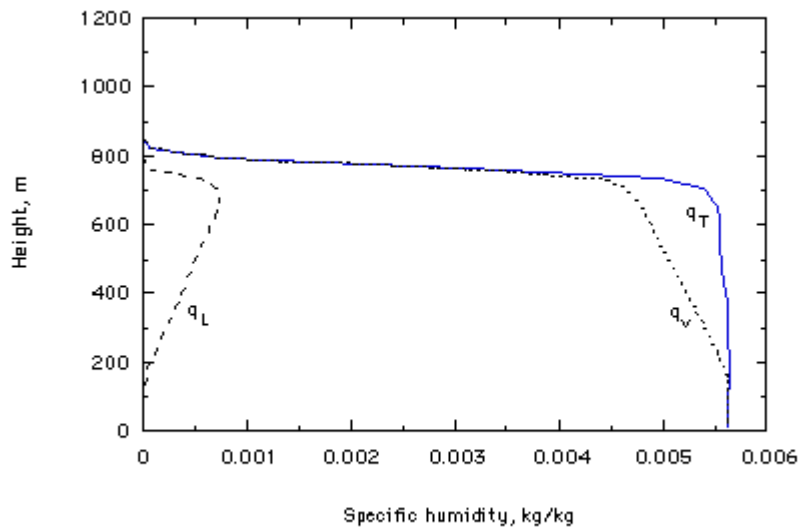


Figure 5. Vertical profiles of the total water content q_T , liquid water content q_L , and water vapor specific humidity q_v , for the CTBL simulation.

The temperature fields of the virtual potential temperature, and the potential liquid water temperature are shown in Figure 3. As expected, the potential liquid water temperature is constant in the mixed layer. The turbulent heat flux and the net radiative flux are shown in Figure 4. The net radiative flux is prescribed in this study as decreasing from 0.07 K m/s to zero within the top 200 m of the cloud. The radiative flux is the driving force of the generated convection. In our simulation, its divergence is equivalent to a minimum cooling of about 2.5 K/h in the cloud layer. In Figure 4, the sum of the radiative and turbulent fluxes is linear in the mixed layer, which indicates a quasi steady state.

Humidity fields of total water content, the liquid water content, and water vapor specific humidity are presented in Figure 5. The liquid water content in Figure 5 indicates that the cloud extends from 200 to 800 m. As expected, the total water content is constant in the mixed layer.

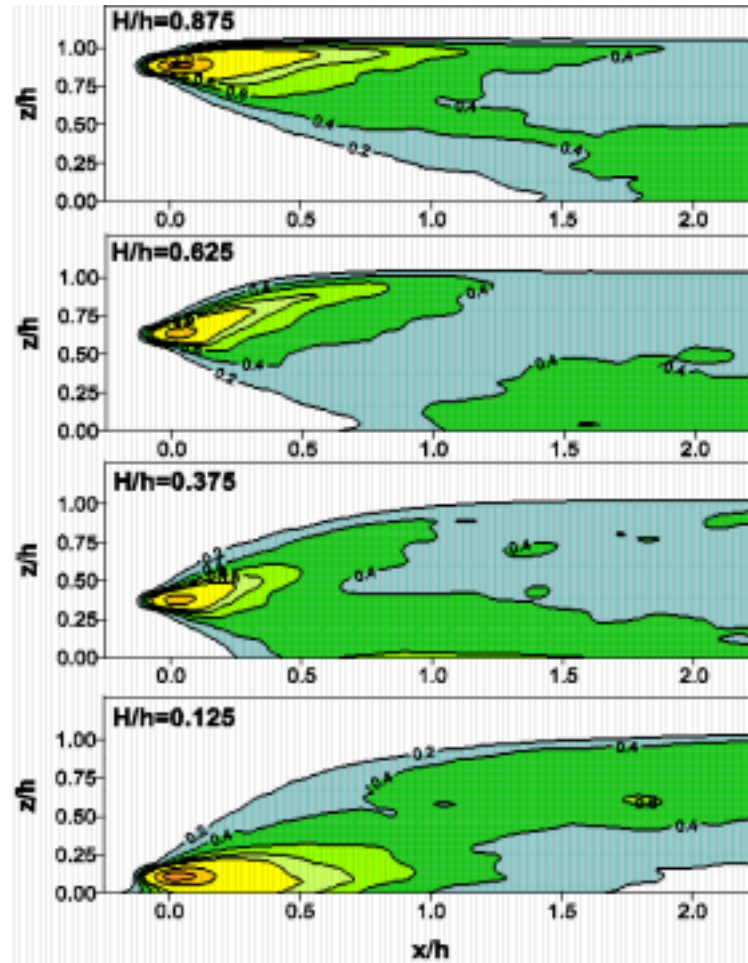


Figure 6. Normalized cross-wind integrated concentrations, $\langle C \rangle y h U/Q$, for a tracer released from four point emission sources located at height 100, 300, 500, 700 m above the ground surface

3.4. Resulting concentration fields

We simulated tracer releases from four point sources located at different heights within the mixed layer: $H=100$ m ($H/h=0.125$), $H=300$ m ($H/h=0.375$), $H=500$ m ($H/h=0.625$), and $H=700$ m ($H/h=0.875$). The LES model was restarted after 15,136 s and ran together with the Lagrangian particle model for the next 1500 time steps. The ensemble mean concentrations were calculated as described in section 3.2, on a grid with the same resolution as the LES model grid. The resulting cross-wind integrated concentrations (CWIC) are displayed in Figure 6. The corresponding dimensionless mean plume heights are presented in Figure 7. They are defined as $Z=\langle Cz \rangle / \langle C \rangle$, where $\langle \rangle$ denotes the vertical and lateral averaging operator.

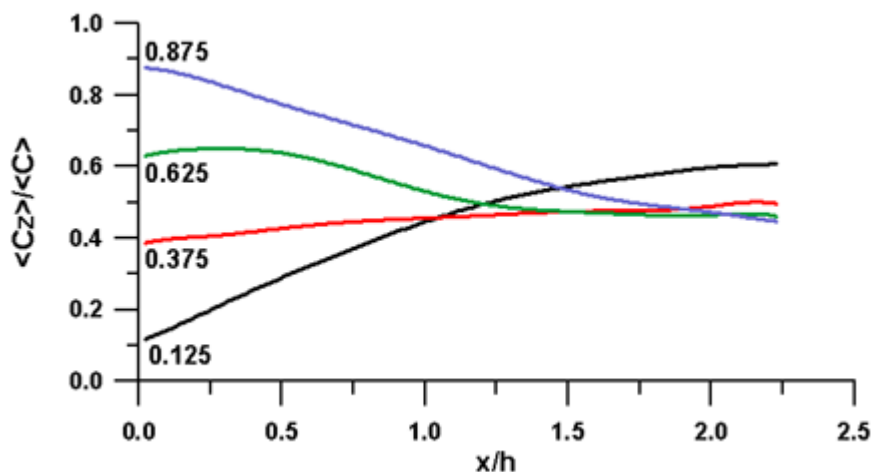


Figure 7. Dimensionless mean plume heights corresponding to the concentrations in Figure 6.

The plume released from the lowest source ($H/h=0.125$) ascends. This happens because the material released at the surface can only ascend or move horizontally. The contaminants released into the base of an updraft rise immediately, while those emitted into a downdraft move approximately horizontally, until they encounter updrafts. This plume behavior is similar to that observed in the clear-sky CBL.

In the case of elevated sources located in the middle of the mixed layer ($H/h=0.375$ and $H/h=0.625$), the plumes start to ascend immediately after the release. This is consistent with the negative skewness of vertical velocity obtained from the LES (Figure 2). The considered plumes encounter stronger narrow downdrafts surrounded by larger areas of weaker updrafts and, consequently, the majority of the released tracer ascends. This is the opposite situation to the case of elevated release in the clear-sky CBL. The ascending of the plume released from the highest source ($H/h=0.875$) is limited by the inversion top.

It is interesting to note the plume splitting which occurs in further distances from the elevated sources. In each case, a portion of the plume starts descending and continues to descend until it reaches the ground surface. Another portion keeps ascending or moves horizontally. This plume splitting explains why the ascend of the elevated plumes is not clearly visible in the mean plume heights in Figure 7. All plumes released from both, surface and elevated sources cross approximately at $Z = 0.5$ and $x/h = 1.5$. Since, the maximum concentration does not stay at the same level (except at larger distances from the source), and all

plumes experience a certain degree of splitting with travel time, we conclude that the obtained dispersion patterns are different from those produced by the Gaussian plume models.

4. FINAL REMARKS

Current regulatory practice in air pollution modeling adopts the Gaussian plume equation, and assumes dispersion parameters to be defined for six classes of atmospheric stability: from extremely unstable (class A) to moderately stable (class F). At night with low clouds, the scheme yields neutral or lightly stable classes D and E. Our study shows that in such conditions, convection can occur in the nocturnal boundary layer, and that the Pasquill-Turner classification is not valid. The performed simulations also demonstrate that vertical diffusion in the nocturnal CTBL is non-Gaussian. Both conclusions imply the need for a revised formulation of diffusion models in a nocturnal CTBL, with upgraded dispersion parameters, and improved treatment of plume rise and buoyancy effects. Related issues are addressed by Pielke and Uliasz (1998), who discussed the limitations and strengths of available meteorological models for atmospheric dispersion applications.

The presented results are based on large-eddy simulations, and therefore are merely preliminary in character. Obviously, further experimental verification is required. We hope to test our findings during the CASES-99 experiment planned to take place in Kansas in the fall of 1999. One of the goals during this project will be a study of diffusion under cloudy skies at night. During the experiment aerosol will be generated at various heights in the nocturnal boundary layer and its dispersion detected by means of lidar measurements.

5. REFERENCES

- Beets C., and B. Koren, 1996: Large-eddy simulation with accurate implicit subgrid-scale diffusion. Department of Numerical Mathematics. Centrum voor Wiskunde en Informatica. Report NM-R9601, January 1996.
- Cuijpers J.W.M., and P.G. Duynkerke, 1993: Large-eddy simulation of trade wind cumulus clouds. *J. Atmos. Sci.*, 50, 3894-3908.
- Deardorff, J. W., 1972: Numerical integration of neutral and unstable planetary boundary layers. *J. Atmos. Sci.*, 29, 91-115.
- Deardorff, J. W., 1973: Three-dimensional numerical modeling of the planetary boundary layers. Workshop on Micrometeorology, D.A. Haugen, Ed., Amer. Meteor. Soc., 271- 311.
- Deardorff, J. W., 1974: Three-dimensional numerical study of turbulence in an entraining mixed layer. *Bound.-Layer Meteor.*, 7, 199-226.
- Deardorff, J.W., 1976: On the entrainment rate of a stratocumulus-topped mixed layer. *Quart. J. Roy. Meteor Soc.*, 102, 563-582.
- Deardorff, J. W., 1980: Stratus-capped mixed layers derived from a three-dimensional model. *Bound.-Layer Meteor.*, 18, 495-527.
- Eberhart, W.L., W.R. Moninger, and G.A. Briggs, 1988: Plume dispersion in the convective boundary layer. Part I: CONDORS field experiment and example measurements. *J. Appl. Meteor.*, 27, 5, 600-616
- Garratt, J.R., 1992: The atmospheric boundary layer. Cambridge University Press.
- Lamb R.G., 1982: A numerical simulation of dispersion from an elevated point source in the convective planetary boundary layer. *Atmos. Envir.* 12, 1297-1304.
- LeMone, M.A., 1990: Some observations of vertical velocity skewness in the planetary boundary layer. *J. Atmos. Sci.*, 47, 1163-1169.

- Lenschow, D.H., J.C.Wyngaard, W.T.Pennell, 1980: Mean-field and second-moment budgets in a baroclinic, convective boundary layer. *J. Atmos. Sci.*, 37, 1313-1326.
- Lewellen, D.C., and W.S. Lewellen, 1996: Influence of Bowen ratio on boundary layer cloud structure. *J. Atmos. Sci.*, 53, 175-187.
- Mason, P.J., 1989: Large-eddy simulation of the convective atmospheric boundary layer. *J. Atmos. Sci.*, 46, 1492-1516.
- Mason, P.J., 1994: Large-eddy simulation: A critical review of the technique. *Quart. J. Roy. Meteor. Soc.*, 120, 1-26.
- Moeng C.-H., and R. Rotunno, 1990: Vertical-velocity skewness in the buoyancy driven boundary layer. *J. Atmos. Sci.*, 47, 1149-1162.
- Moeng, C.-H., 1984: A large-eddy simulation model for the study of planetary boundary-layer turbulence. *J. Atmos. Sci.*, 41, 2052-3169.
- Moeng, C.-H., 1986, Large-eddy simulation of a stratus-topped boundary Part I: Structure and budgets. *J. Atmos. Sci.*, 43, 2886-2900.
- Moeng, C.-H., W.R. Cotton, C. Bretherton, A. Chlond, M. Khairoutdinov, S. Krueger, W.S. Lewellen, M.K. MacVean, J.R.M. Pasquier, H.A. Rand, A.P. Siebesma, B. Sievers, and R.I. Sykes, 1996: Simulation of a stratocumulus-topped planetary boundary layer: Intercomparison among Different numerical codes. *Bull. Amer. Meteor. Soc.*, 77, 261-278.
- Moninger, W.R., and R.A. Kropfli, 1982: Radar observations of a plume from an elevated continuous point source. *J. Appl. Meteor.*, 21, 11, 1685-1697
- Nieuwstadt, F.T.M., 1990: Direct and large-eddy simulation of free convection. *Pro. Thea Into. Heat Transfer Con.*, Jerusalem, vol.1, Amer. Soc. Much. Engr., pp. 37-47.
- Nieuwstadt, F.T.M., P.J. Mason, C. H. Moeng, and U. Schumann, 1992: Large-eddy simulation of convective boundary-layer: A comparison of four computer codes. *Turbulent Shear Flows 8*, Dust H. et al., Ens, Springer-Verlag, 343-367.
- Nichols S., 1989: The structure of radiatively driven convection in stratocumulus. *Quart. J. R. Meteor. Soc.*, 115, 487-511.
- Nichols S., and J. Leighton, 1986: An observational study of the structure of stratiform cloud sheets: Part I: Structure. *Q. J. R. Meteor. Soc.* 112, 431-460.
- Paluch I.R., and D.H. Lenchow, 1991: Stratiform cloud formation in the marine boundary layer. *J. Atmos. Sci.*, 48, 2141-2158.
- Pielke, R.A. and M. Uliasz, 1998: Use of meteorological models as input to regional and mesoscale air quality models: Limits and strengths. *Atmos. Envir.*, 32, 1455-1466.
- Sawford, B.L., and F.M. Guest, 1987: Lagrangian stochastic analysis of flux-gradient relationships in the convective boundary layer. *J. Atmos. Sci.*, 44, 1152-1165.
- Schemm, C. E., and F. B. Lipps, 1976: Some results from a simplified three-dimensional numerical model of atmospheric turbulence. *J. Atmos. Sci.*, 33, 1021-1041.
- Schmidt, H., and U. Schumann, 1989: Coherent structure of the convective boundary layer derived from large-eddy simulation. *J. Fluid Mech.*, 200, 511-562.
- Sommeria, G., 1976: Three-dimensional simulation of turbulent processes in an undisturbed trade wind boundary layer. *J. Atmos. Sci.*, 33, 216-241.
- Sorbjan, Z., 1995: Toward evaluation of heat fluxes in the convective boundary layer. *J. Appl. Meteor.*, 34, 1092-1098
- Sorbjan, Z., 1996 a, Numerical study of penetrative and "solid-lid" non-penetrative convective boundary layers. *J. Atmos. Sci.*, 53, 101-112.
- Sorbjan, Z., 1996 b: Effects caused by varying strength of the capping inversion based on a large-eddy simulation of the shear-free convective boundary layer. *J. Atmos. Sci.*, 53, 2015-2024.
- Turton J., and S. Nicholls, 1987: A study of the diurnal variation of stratocumulus using a multiple mixed-layer model. *Q. J. R. Meteor. Soc.* 113, 969-1011.
- Uliasz, M., 1994: Lagrangian particle modeling in mesoscale applications. *Environmental Modeling II*, ed. P. Zannetti, Computational Mechanics Publications, 71-102.

- Uliasz, M., R.A. Stocker, and R.A. Pielke, 1996: Regional modeling of air pollution transport in the southwestern United States. *Environmental Modeling III*, ed. P. Zannetti, Computational Mechanics Publications, 145-182.
- Weil, J.C., 1988: Dispersion in the convective boundary layer. In: *Lectures on Air Pollution*, AMS, 390 pp.
- Willis, G.E., and J.W. Deardorff, 1976: A laboratory model of diffusion into the convective planetary boundary layer. *Quart.J.Roy.Met.Soc.*, 102, 427-445
- Willis G.E., and J.W. Deardorff 1978 A laboratory study of dispersion from an elevated source within a modeled convective planetary boundary layer. *Atmos. Envir.* 12, 1305-1312.
- Willis, G.E., and J.W. Deardorff, 1981: A laboratory study of dispersion from a source in the middle of the convectively mixed layer. *Atmos. Envir.* 15, 109-117.
- Yeung P.K. and S. B. Pope, 1988: An algorithm for tracking fluid particles in numerical simulations of homogeneous turbulence. *J. Comput. Physics*, 79, 373-416.